JOURNAL OF MATERIALS SCIENCE 31 (1996) 2027–2034

Reduction in energy release rate for mode I fracture of a fibre with a cracked coating layer due to small-scale interfacial debonding

S. OCHIAI, M. HOJO
Mesoscopic Materials Research Center, Faculty of Engineering, Kyoto University, Sakyo-ku, Kyoto 606, Japan

In order to predict the effect of small-scale interfacial debonding on the energy release rate at a crack tip for mode I fracture of a fibre with a cracked coating layer, an approximate calculation method has been presented. The relation of debonding length, thickness of the coating layer and ratio of elastic modulus of the coating layer to that of the fibre, to the energy release rate of the fibre was calculated for some examples. It was demonstrated that small-scale debonding reduces the energy release rate and, therefore, effectively prevents reduction in fibre strength.

1. Introduction

When a fibre is coated with low-failure-strain material, the strength is sometimes reduced. One of the reasons for the reduction could be attributed to the propagation of the crack formed by premature fracture of the coating layer [1–6]. In this case, if the interfacial bonding strength between fibre and coating layer is high, the formed notch extends into the fibre, and the fibre is broken in Mode I, as schematically shown in Fig. 1a. As a result, the strength of the fibre is seriously reduced. On the other hand, if the bonding strength is low, debonding occurs at the interface, as shown in Fig. 1b. In this case, the crack-tip is blunted and the reduction in fibre strength is not serious [3, 7]. However, if debonding occurs in a large scale along the length, the efficiency of stress transfer from matrix to fibre becomes low when fibres are embedded in a matrix, resulting in a low strength of composites [8, 9]. Thus, in order to prevent reduction in fibre strength and also to retain high efficiency of stress transfer in composites, small-scale debonding is required.

Although the importance of small-scale debonding has been recognized in this field, the relation of debonding length to fibre strength has not been clarified until now. In the present paper, in order to predict the energy release rate for mode I fracture of a fibre at the crack tip after small-scale interfacial debonding, an approximate calculation method will be presented. Some calculation results concerning the dependences of the energy release rate on debonding length, thickness of the coating layer and elastic moduli of fibre and coating layer, will be shown.

2. Calculation method

2.1. Relationship of energy release rate to compliance

The strain energy release rate of a fibre, λ, is given by [10]

$$\lambda = (P^2/2)\,[\mathrm{d}C(S)/\mathrm{d}S] \quad (1)$$

where P is the applied load, $C(S)$ is the compliance for crack of area S and $\mathrm{d}S$ is the increment of cross-sectional area of the crack. In this work, λ is calculated by modifying Equation 1 into the form

$$\lambda = (P^2/2)\left\{\lim_{\Delta S \to 0} [C(S + \Delta S) - C(S)]/(\Delta S)\right\} \quad (2)$$

The $C(S)$ and $C(S + \Delta S)$ are calculated by the method shown in Section 2.2, and fracture of the fibre is regarded to occur when

$$\lambda \geqslant \lambda_c \quad (3)$$

where λ_c is the critical strain energy release rate.

2.2. Modelling

The shear-lag analysis technique has been known to be useful to calculate stress concentrations in the fibres adjacent to broken fibres in fibre-reinforced composites [11–15]. This technique has also been applied successfully to calculate the energy release rates for modes I and II for notched multifibre-reinforced plastics by Narin [16] and for a single-fibre composite in which a broken fibre is embedded in a matrix, by Fukuda [17]. In this analysis technique, the stress distribution in the longitudinal direction is calculated by ignoring radial and circumferential

0022–2461

stresses. On this point, this technique is not rigid. However, for approximate estimation, it is known to be useful. Also it has the advantage that the calculation procedure is simple. In this work, this technique is extended for the following model coated fibre.

The fibre has a radius R_f and length L which is taken to be infinite in the calculation, cross-sectional area S_f, Young's and shear moduli E_f and G_f, respectively, and the coating layer has an outer radius R_c, cross-sectional area S_c, Young's and shear moduli, E_c and G_c, respectively. The coating layer with a thickness $a(=R_c - R_f)$ is broken at $X = 0$, as shown in Fig. 1a. Between Young's, E, and shear, G, moduli, the relation

$$G = E/[2(1 + \nu)] \quad (4)$$

is assumed, where ν is the Poisson's ratio.

Let us consider the situation where debonding has occurred by D in length below and above the crack. There are two regions, as schematically shown in Fig. 1b: region A($X \geqslant D$) where coating layer adheres to the fibre, and region B ($0 \leqslant X \leqslant D$) where interfacial debonding has occurred. When interfacial bonding is strong, region B does not exist and only region A exists, as shown in Fig. 1a.

The fibre and coating layer are regarded to be composed of $N1$ and $N2$ elements, respectively, as shown in Fig. 2a. The total number of elements is $N(=N1 + N2)$. The element in the centre is numbered 1, the next one 2, and then 3, 4, ... , N outwards. The cross-sectional area of the i element is given by S_i. The interface between $i - 1$ and i elements is expressed as the $i - 1/i$ interface. The outer and inner radii of the ith element are denoted R_i and R_{i-1}, respectively, and the distance of the centroid from the inner surface of ith element as C_i, as shown in Fig. 2b. The displacement from $X = 0$ of the ith element is denoted U_i and that of the interface between $i - 1$ and i as $U_{i-1/i}$. The Young's and shear moduli of the ith element are shown by E_i and G_i, respectively. If the ith element exists within the fibre, E_i and G_i are given by E_f and G_f, respectively, while, if it exists within the coating, they are given by E_c and G_c, respectively.

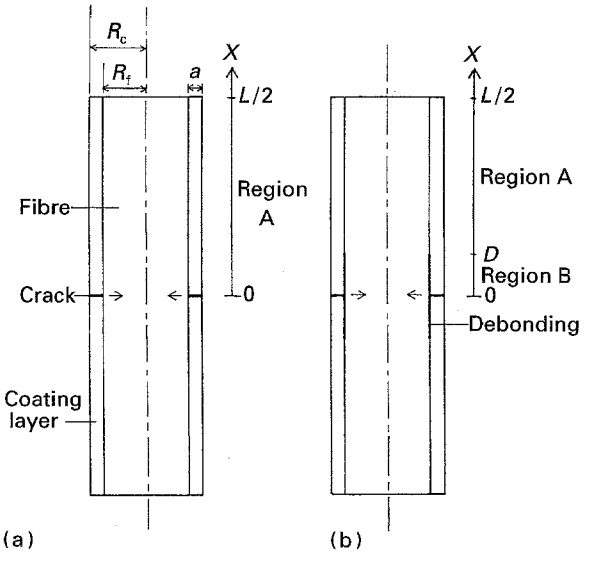

Figure 1 Schematic representation of the non-debonded (A) and the debonded (B) regions. The arrows show the direction of the crack propagation. (a) and (b) correspond to the cases without and with interfacial debonding between fibre and coating layer, respectively.

2.3. Equations for stress equilibrium

For Region A, the interfacial shear stress at the $i/i + 1$ interface, $\tau_{i/i+1}$, is approximately given by [18]

$$\tau_{i/i+1} = G_i(U_{i/i+1} - U_i)/(R_i - C_i - R_{i-1}) = G_{i+1}(U_{i+1} - U_{i/i+1})/C_{i+1} \quad (5)$$

Eliminating $U_{i/i+1}$ in Equation 5, we have

$$\tau_{i/i+1} = H_i(U_{i+1} - U_i) \quad (6)$$

$$H_i = G_iG_{i+1}/[G_iC_{i+1} + G_{i+1}(R_i - C_i - R_{i-1})] \quad (7)$$

For region B, the shear stress $\tau_{i/i+1}$ for $i \neq N1$ is also given by Equation 5, and the shear stress $\tau_{N1/N1+1}$ is given by zero. The forces acting on the ith element are shown in Fig. 2b where P_i is the load at $X = X$ in the longitudinal direction. The equations for stress equilibrium for regions A and B are given as follows.

Region A

$$S_1E_1(d^2U_1/dX^2) + 2\pi R_1\tau_{1/2} = 0 \quad (8)$$

$$S_iE_i(d^2U_i/dX^2) + 2\pi(R_i\tau_{i/i+1} - R_{i-1}\tau_{i-1/i}) = 0 \ (i = 2 \text{ to } N - 1) \quad (9)$$

$$S_NE_N(d^2U_N/dX^2) - 2\pi R_{N-1}\tau_{N-1/N} = 0 \quad (10)$$

Region B

$$S_1E_1(d^2U_1/dX^2) + 2\pi R_1\tau_{1/2} = 0 \quad (11)$$

$$S_iE_i(d^2U_i/dX^2) + 2\pi(R_i\tau_{i/i+1} - R_{i-1}\tau_{i-1/i}) = 0 \ (i = 2 \text{ to } N1 - 1) \quad (12)$$

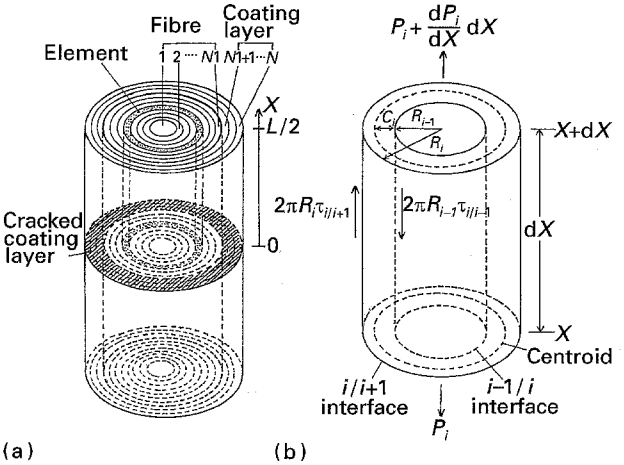

Figure 2 (a) Modelling for application of shear lag analysis. The fibre and coating layer are divided into $N1$ and $N2$ cylindrical elements, respectively. (b) Equilibrium of force in the ith element.

$$S_{N1}E_{N1}(d^2U_{N1}/dX^2) + 2\pi$$
$$(-R_{N1-1}\tau_{N1-1/N1}) = 0 \quad (13)$$
$$S_{N1+1}E_{N1+1}(d^2U_{N1+1}/dX^2) + 2\pi$$
$$(R_{N1+1}\tau_{N1+1/N1+2}) = 0 \quad (14)$$
$$S_iE_i(d^2U_i/dX^2) + 2\pi$$
$$(R_i\tau_{i/i+1} - R_{i-1}\tau_{i-1/i}) = 0$$
$$(i = N1+2 \text{ to } N-1) \quad (15)$$
$$S_NE_N(d^2U_N/dX^2) + 2\pi(-R_{N-1}\tau_{N-1/N}) = 0 \quad (16)$$

2.4. Non-dimensionallization

In order to obtain a convenient form for the problem, a non-dimensionallization has been performed in the shear lag analysis [11–17]. In this work, the ordinary expression of non-dimensionallization was modified for the present problem as follows

$$R_i = R_f r_i \quad (17)$$
$$C_i = R_f c_i \quad (c_i = [(r_i^2 + r_{i-1}^2)/2]^{1/2} - r_{i-1}) \quad (18)$$
$$S_i = S_f s_i = \pi R_f^2 s_i \quad (19)$$
$$E_i = E_f e_i \quad (20)$$
$$G_i = G_f g_i \quad (21)$$
$$H_i = G_f h_i / R_f$$
$$(h_i = g_i g_{i+1}/[g_i c_{i+1} + g_{i+1}(r_i - c_i - r_{i-1})]) \quad (22)$$
$$U_i(i = 1 \text{ to } N) = \sigma_f R_f\{1/(E_f G_f)\}^{1/2} u_i \quad (23)$$
$$X = R_f(E_f/G_f)^{1/2}x \quad (24)$$
$$L = R_f(E_f/G_f)^{1/2}l \quad (25)$$
$$D = R_f(E_f/G_f)^{1/2}d \quad (26)$$

where σ_f is the average fibre stress at $X = 0$ (= net fibre stress). r_i, c_i, s_i, e_i, g_i, h_i, u_i, x, l and d are non-dimensionallized forms of R_i, C_i, S_i, E_i, G_i, H_i, U_i, X, L and D, respectively.

Under this non-dimensionallization, $du_i(x)/dx$ (denoted $K_i(x)$) is given by

$$K_i(x) = du_i/dx = \{dU_i(X)/dx\}/(\sigma_f/E_f) \quad (27)$$

Equation 27 shows that $K_i(x)$ is the magnitude of strain normalized with respect to the average strain of a fibre at $x = 0$. Substituting Equations 17–26 into Equations 8–16, and letting

$$2r_ih_i/(e_is_i) = m_i \quad (28)$$
$$2r_{i-1}h_{i-1}/(e_is_i) = n_i \quad (29)$$

we have following simplified equations.

Region A

$$d^2u_1/dx^2 + m_1(u_2 - u_1) = 0 \quad (30)$$
$$d^2u_i/dx^2 + m_iu_{i+1} - (m_i + n_i)u_i + n_iu_{i-1} = 0$$
$$(i = 1 \text{ to } N-1) \quad (31)$$
$$d^2u_N/dx^2 - n_N(u_N - u_{N-1}) = 0 \quad (32)$$

Region B

$$d^2u_1/dx^2 + m_1(u_2 - u_1) = 0 \quad (33)$$
$$d^2u_i/dx^2 + m_iu_{i+1} - (m_i + n_i)u_i + n_iu_{i-1} = 0$$
$$(i = 2 \text{ to } N1-1) \quad (34)$$
$$d^2u_{N1}/dx^2 - n_{N1}(u_{N1} - u_{N1-1}) = 0 \quad (35)$$
$$d^2u_{N1+1}/dx^2 + m_{N1+1}(u_{N1+2} - u_{N1+1}) = 0 \quad (36)$$
$$d^2u_i/dx^2 + m_iu_{i+1} - (m_i + n_i)u_i + n_iu_{i-1} = 0$$
$$(i = N1+2 \text{ to } N-1) \quad (37)$$
$$d^2u_N/dx^2 - n_N(u_N - u_{N-1}) = 0 \quad (38)$$

2.5. General solution of u_i

When L is taken to be large enough, the strain of all elements $dU_i(X)/dX$ at $X = L/2$ are equal to each other, given by

$$dU_i(X = L/2)/dX = R_f^2\,\sigma_f/[R_f^2E_f + (R_c^2 - R_f^2)E_c] \quad (39)$$

Substituting Equation 39 into Equation 27, we have

$$K_i(X = L/2) = R_f^2/[R_f^2 + (R_c^2 - R_f^2)(E_c/E_f)]$$
$$(i = 1 \text{ to } N) \quad (40)$$

The general solutions of u_is for regions A and B are given as follows under the condition of Equation 40.

Region A

$$u_i^A = \sum_{j=1}^{N-1} A_jB_{i,j}\exp(-k_jx) + \{R_f^2/[R_f^2 + (R_c^2 - R_f^2)(E_c/E_f)]\}x + A_N \quad (41)$$

where A_js are unknown constants, $(k_j)^2$s $(k_j > 0)$ are eigen values except zero for the matrix $\boldsymbol{T}_N$ given by

$$\boldsymbol{T}_N = \begin{bmatrix} m_1 & -m_1 & & & & \\ -n_2 & m_2+n_2 & -m_2 & & 0 & \\ & -n_3 & m_3+n_3 & -m_3 & & \\ & \cdots & \cdots & \cdots & \cdots & \\ & & & -n_{N-1} & m_{N-1}+n_{N-1} & -m_{N-1} \\ & 0 & & & -n_N & n_N \end{bmatrix} \quad (42)$$

and $B_{i,j}$s are constants given by

$$B_{1,j} = 1 \quad (j = 1 \text{ to } N-1) \tag{43}$$

$$B_{2,j} = (1 - k_j^2/m_1)B_{1,j} \quad (j = 1 \text{ to } N-1) \tag{44}$$

$$B_{i,j} = (1 + n_{i-1}/m_{i-1} - k_j^2/m_{i-1})\,B_{i-1,j} - (n_{i-1}/m_{i-1})B_{i-2,j} \quad (i = 3 \text{ to } N, j = 1 \text{ to } N-1) \tag{45}$$

Region B

$$u_i^B = \sum_{j=1}^{2(N_{1-1})} C_j D_{i,j} \exp(v_j x) + C_{2N1-1}x + C_{2N1} \quad (i = 1 \text{ to } N1 \text{ (fibre elements)}) \tag{46}$$

$$u_i^B = \sum_{j=2N1+1}^{2N1+2(N2-1)} C_j D_{i,j} \exp\{w_j x\} + C_{2N-1}x + C_{2N} \quad (i = N1+1 \text{ to } N \text{ (coating elements)}) \tag{47}$$

where C_js are unknown constants, $(v_j)^2$s and $(w_j)^2$s are eigen values except zero for the following matrices $\boldsymbol{T}_{N1}$ and $\boldsymbol{T}_{N2}$, respectively.

$$\boldsymbol{T}_{N1} = \begin{bmatrix} m_1 & -m_1 & & & & \\ -n_2 & m_2+n_2 & -m_2 & & 0 & \\ & -n_3 & m_3+n_3 & -m_3 & & \\ \cdots & \cdots & \cdots & \cdots & \cdots & \cdots \\ & & & -n_{N1-2} & m_{N1-2}+n_{N1-2} & -m_{N1-2} \\ & 0 & & & -n_{N1-1} & n_{N1-1} \end{bmatrix} \tag{48}$$

$$\boldsymbol{T}_{N2} = \begin{bmatrix} m_{N1+1} & -m_{N1+1} & & & & \\ -n_{N1+2} & m_{N1+2}+n_{N1+2} & -m_{N1+2} & & 0 & \\ & -n_{N1+3} & m_{N1+3}+n_{N1+3} & -m_{N1+3} & & \\ \cdots & \cdots & \cdots & \cdots & \cdots & \cdots \\ & & & -n_{N-1} & m_{N-1}+n_{N-1} & -m_{N-1} \\ & 0 & & & -n_N & n_N \end{bmatrix} \tag{49}$$

and $D_{1,j}$s are constants given by

$$D_{1,j} = 1 \ (j = 1 \text{ to } 2(N1-1)) \tag{50}$$

$$D_{2,j} = (1 - v_j^2/m_1)D_{1,j} \quad (j = 1 \text{ to } 2(N1-1)) \tag{51}$$

$$D_{i,j} = (1 + n_{i-1}/m_{i-1} - v_j^2/m_{i-1})\,D_{i-1,j} - (n_{i-1}/m_{i-1})D_{i-2,j} \quad (i = 3 \text{ to } N1,\ j = 1 \text{ to } 2(N1-1)) \tag{52}$$

$$D_{N1+1,j} = 1 \quad (j = 2N1+1 \text{ to } 2N1+2(N2-1)) \tag{53}$$

$$D_{N1+2,j} = (1 - w_j^2/m_{N1+1})\,D_{N1+1,j} \quad (j = 2N1+1 \text{ to } 2N1+2(N2-1)) \tag{54}$$

$$D_{i,j} = (1 + n_{i-1}/m_{i-1} - w_j^2/m_{i-1})\,D_{i-1,j} - (n_{i-1}/m_{i-1})D_{i-2,j} \quad (i = N1+3 \text{ to } N, j = 2N1+1 \text{ to } 2N1+2(N2-1)) \tag{55}$$

2.6. Boundary conditions

The unknown constants, A_js ($j = 1$ to N) in the case of no debonding, and A_js ($j = 1$ to N) and C_js ($j = 1$ to $2N$) in the case of debonding, could be solved from the following boundary conditions. For the present aim, the following situations (i)–(iii) were taken for the reason given later. In this section, only the conditions for the case of debonding are shown. For the case of no debonding, the same conditions can be used by setting $d = 0$.

Situation (i): no fibre elements are broken

$$u_i^B(0) = 0 \text{ for } i = 1 \text{ to } N1 \tag{56}$$

$$K_i^B(0) = 0 \text{ for } i = N1+1 \text{ to } N \tag{57}$$

$$u_i^B(d) = u_i^A(d) \text{ for } i = 1 \text{ to } N \tag{58}$$

$$K_i^B(d) = K_i^A(d) \text{ for } i = 1 \text{ to } N \tag{59}$$

Situation (ii): the fibre element $N1$ is broken

$$u_i^B(0) = 0 \text{ for } i = 1 \text{ to } N1-1 \tag{60}$$

$$K_i^B(0) = 0 \text{ for } i = N1 \text{ to } N \tag{61}$$

Equations 58 and 59.

Situation (iii): the fibre elements $N1$ and $N1-1$ are broken

$$u_i^B(0) = 0 \text{ for } i = 1 \text{ to } N1-2 \tag{62}$$

$$K_i^B(0) = 0 \text{ for } i = N1-1 \text{ to } N \tag{63}$$

Equations 58 and 59.

2.7. Strain energy release rate, λ

Assuming that L is large, $\exp(-k_j l/2)$ in Equation 41 is nearly zero, where l is a non-dimensional form of L given by Equation 25. In such a situation, the non-dimensional displacement of all fibre elements at $x = l/2$ is given by $[R_f^2/\{R_f^2 + (R_c^2 - R_f^2)\ (E_c/E_f)\}]\ (l/2) + A_N$. Denoting the non-dimensional displacement at $x = l/2$ for crack area S as $u(S)$ and the non-dimensional value of A_N for crack area S as $A_N(S)$, $u(S)$ is expressed as

$$u(S) = [R_f^2/\{R_f^2 + (R_c^2 - R_f^2)\ (E_c/E_f)\}]\ (l/2) + A_N(S) \tag{64}$$

The non-dimensional displacement, $u(S)$, is converted to a real one, $U(S)$, via Equation 23 as follows

$$U(S) = u(S)\sigma_f R_f [1/(E_f G_f)]^{1/2} \quad (65)$$

The compliance for crack area S, $C(S)$, is then given by

$$C(S) = 2U(S)/P \quad (66)$$

where P is the applied load. Now let the crack propagate by ΔS. For crack area $S + \Delta S$, the compliance $C(S + \Delta S)$ is given by

$$C(S + \Delta S) = 2U(S + \Delta S)/P \quad (67)$$

Setting $P = \pi R_f^2 \sigma_f$ and combining Equations 23, 64–67 with Equation 2, we have

$$\lambda/\sigma_f^2 = \pi R_f^2 [1/(E_f G_f)]^{1/2} \left(\lim_{\Delta S \to 0} \pi R_f \{[A_N(S + \Delta S) - A_N(S)]/\Delta S\} \right) \quad (68)$$

λ/σ_f^2 is independent of σ_f. In the present work, λ/σ_f^2 was calculated as follows. S was taken to be the cross-sectional area of the coating layer and $A_N(S)$ was calculated by using the boundary conditions for Situation (i). Next, ΔS (described as ΔS_1) was taken to be the cross-sectional area of $N1$ element ($\Delta S_1 = S_{N1}$), and the unknown constant $A_N(S + \Delta S_1)$ was obtained by using the boundary conditions for Situation (ii). Then $\Delta S(\Delta S_2)$ were taken to be the sum of the cross-sectional area of $N1$ and $N1 - 1$ elements and the unknown constant $A_N(S + \Delta S_2)$ was obtained by using the boundary conditions for Situation (iii). The value of λ/σ_f^2 was calculated from Equation 68 with the linear extrapolation of $[A_N(S + \Delta S) - A_N(S)]/\Delta S$ to $\Delta S = 0$.

In the present work, R_f was taken to be 5 μm, and a and D were varied up to 1 and 3 μm, respectively. The calculation was carried out for the combinations of (A) $E_f = 200$ GPa and $E_c = 400$ GPa and (B) $E_{if} = 400$ GPa and $E_c = 200$ GPa. The former represents the case where the coating layer has higher elastic modulus than the fibre and the latter the reverse case. For calculation of fibre stress at which the crack propagates into the fibre at $X = 0$, λ_c was taken to be 3 J/m^{-2}. The Poisson's ratios of both fibre and coating layer were assumed to be 0.3. $N1$, $N2$ and $S_i (i = 1$ to $N)$ were taken as follows, due to the limiting capacity of the computer used. N_2 was taken to be 12. $N1$ was taken to be the integer of $R_f^2 N2/[(R_f + a)^2 - R_f^2]$ when $R_f^2 N2/[(R_f + a)^2 - R_f^2] < 41$ and 41 when $R_f^2 N2/[(R_f + a)^2 - R_f^2] > 41$. In both cases, S_i was taken to be equal for $i = 2$ to N and S_1 was taken to be the residual. This kind of simplification in the shear-lag analysis has been known to give a fairly good description of stress concentrations at a notch tip [13, 14].

4.

4.1. Influence of interfacial debonding on energy release rate at $X = 0$

Fig. 3 shows the influence of interfacial debonding length on the variation of λ/σ_f^2 at $X = 0$ as a function of a for case (A) ($E_f = 200$ GPa and $E_c = 400$ GPa). Figs 4 and 5 show the variation of λ/σ_f^2 and the energy release rate, λ, normalized with respect to that for $D = 0$ (no debonding) λ_0, respectively, as a function of D for various combinations of the values of a, E_f and E_c. The following features can be read from Figs 3–5.

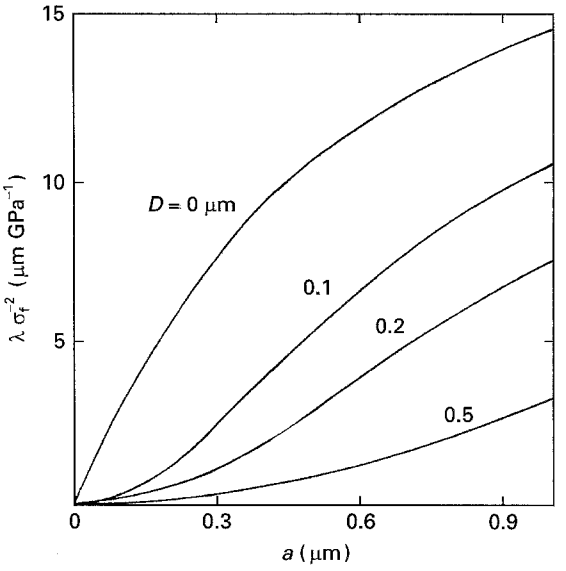

Figure 3 Influence of interfacial debonding length on the variation of λ/σ_f^2 at $X = 0$ as a function of thickness of the coating layer, a, for case A ($E_f = 200$ GPa and $E_c = 400$ GPa).

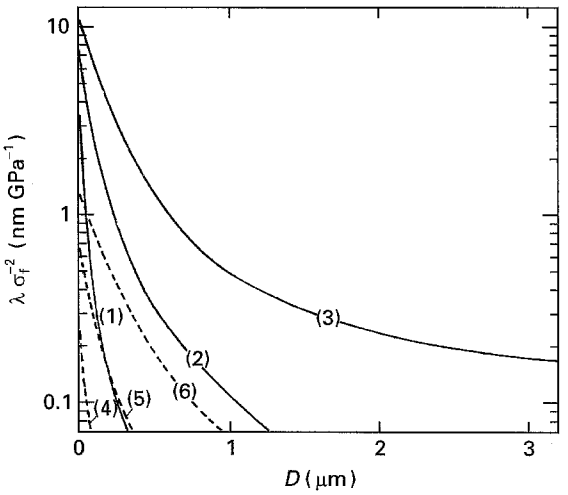

Figure 4 Variation of λ/σ_f^2 as a function of debonding length, D, for (1–3) $E_f = 200$ GPa, $E_c = 400$ GPa, (4–6) $E_f = 400$ GPa, $E_c = 200$ GPa. a: (1, 4) 0.1 μm, (2, 5) 0.3 μm, (3, 6) 0.6 μm.

1. For a given thickness, a, the longer the debonding length, D, the smaller becomes λ/σ_f^2; namely, the interfacial debonding reduces the energy release rate at $X = 0$ and the energy release rate is reduced with increasing debonding length. Even when D is small, the energy release rate is reduced effectively.

2. For a fixed interfacial debonding length, the λ/σ_f^2 increases with increasing a. This indicates that when the coating layer is thick, a long debonding length is required to realize much reduction in energy release rate.

3. In case (A) ($E_f = 200$ GPa and $E_c = 400$ GPa), the λ/σ_f^2 at $D = 0$ (no debonding) is high and also it requires long debonding to achieve low energy release rate, while in case (B) ($E_f = 400$ GPa

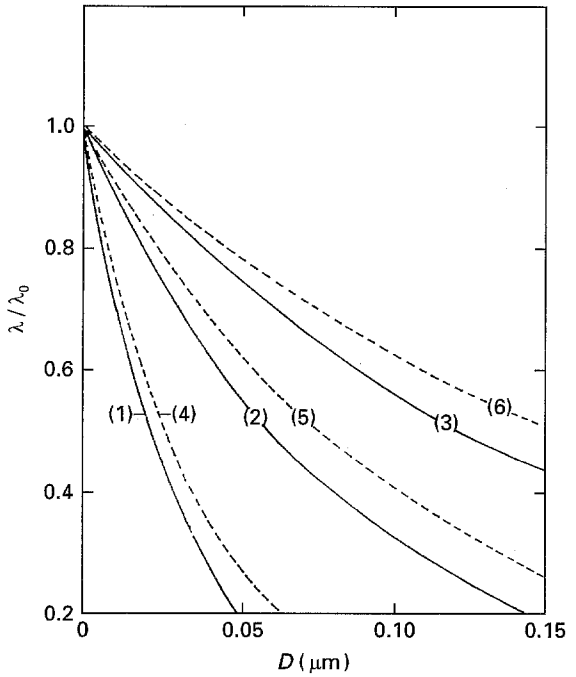

Figure 5 Variation of energy release rate of a fibre at $X = 0$, λ, normalized with respect to that for no debonding ($D = 0$), λ_0, as a function of debonding length D. Curves 1–6 as in Fig. 4.

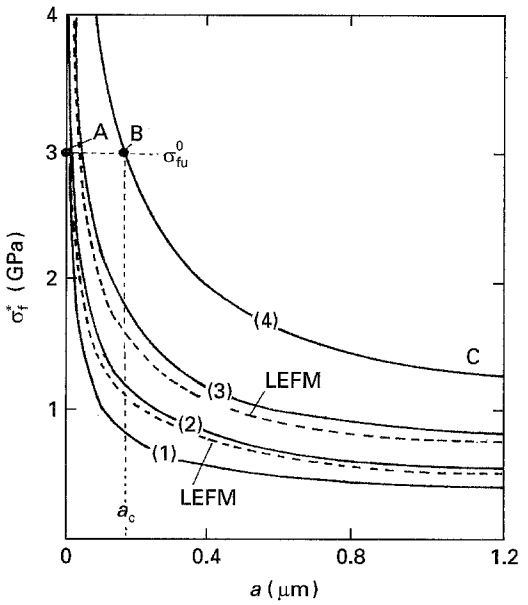

Figure 6 Variation of fibre strength at $X = 0$, σ_f^*, as a function of thickness of the coating layer, a, for the case where no interfacial debonding occurs. (1) $E_f = 200$ GPa, $E_c = 400$ GPa; (4) $E_f = 400$ GPa, $E_c = 200$ GPa. Curves 2 and 3 show the calculation results based on the linear elastic fracture mechanics for the case of $E_c = E_f =$ (2) 200 and (3) 400 GPa. Taking the case of $E_f = 400$ GPa, $E_c = 200$ GPa and an original fibre strength $\sigma_{fu}^0 = 3$ GPa (curve 4) as an example, the practical strength of the fibre at $X = 0$ varies along ABC. In this case, below the critical thickness of the coating layer at B, a_c, the fibre strength at $X = 0$ is given by σ_{fu}^0.

and $E_c = 200$ GPa), the λ/σ_f^2 at $D = 0$ (no debonding) is low and it requires a relatively short debonding length to achieve a low energy release rate. This means that in the case of low-modulus fibre with high-modulus coating layer, the strength is low at $D = 0$ and also even after debonding, the strength cannot become high unless the debonding length becomes long.

4. The relative reduction rate of the energy release rate (λ/λ_0) is high when the thickness of the coating layer is large, E_f is low and E_c is high.

4.2. Stress of the fibre at propagation of the crack at $X = 0$

4.2.1. Stress of the fibre at propagation of the crack at $X = 0$ when no interfacial debonding occurs

Fig. 6 shows the variation of fibre stress, σ_f^*, at which the formed crack propagates into the fibre at $X = 0$. In addition to the variations for cases (A) and (B), the variations for the cases of $E_f = E_c = 200$ and 400 GPa are presented in order to compare the calculation results based on the linear elastic fracture mechanics (LEFM). The following features can be read.

1. According to the LEFM [10], if E_f is equal to E_c, the fibre strength for the plain strain condition will be given by

$$\sigma_f^* = (1/Y)\{E_f\lambda_c/[(1-\nu^2)(\pi a)]\}^{1/2} \quad (69)$$

where Y is the finite width correction factor. The broken curves show the calculation results based on Equation 69. The difference in σ_f^* values between the present method and LEFM is about 10%. This means that the present method is not rigid, but it can be used to a first approximation.

2. In the case of $E_f = E_c$, when the fibre has high elastic modulus, σ_f^* becomes high, as anticipated from Equation 69. It is suggested that if a high-modulus fibre is employed, the reduction in fibre strength is relatively small in comparison with that in low-modulus fibre, if the λ_c value is the same.

3. When a is very small, σ_f^* becomes higher than the original strength (denoted σ_{fu}^0). In such a range of a, the fibre strength is determined by the intrinsic defects contained in the fibre. Then, the strength will not be given by σ_f^* but by σ_{fu}^0. Namely, defining the thickness, which satisfies $\sigma_f^* = \sigma_{fu}^0$, as a_c, the strength will be given by σ_{fu}^0 for $a < a_c$ and by σ_f^* for $a > a_c$. If σ_{fu}^0 is taken to be 3 GPa, the strength for the case of $E_f = 400$ GPa and $E_c = 200$ GPa will not be reduced below the thickness corresponding to B and it will be reduced along BC, as shown in Fig. 6.

4. The strength of fibre is reduced much when E_f is low and E_c is high. On the other hand, the reduction is relatively small when E_f is high and E_c is low. This means that if interfacial bonding is too strong to prevent interfacial debonding, low-modulus fibre with a high-modulus coating layer cannot achieve high strength when the failure strain of the coating layer is very low in comparison with that of the fibre.

4.2.2. Stress of a fibre at propagation of the crack at $X = 0$ when interfacial debonding occurs

Fig. 7 shows the influence of interfacial debonding length D on the variation of fibre stress, σ_f^*, at the propagation of the crack into a fibre at $X = 0$ as

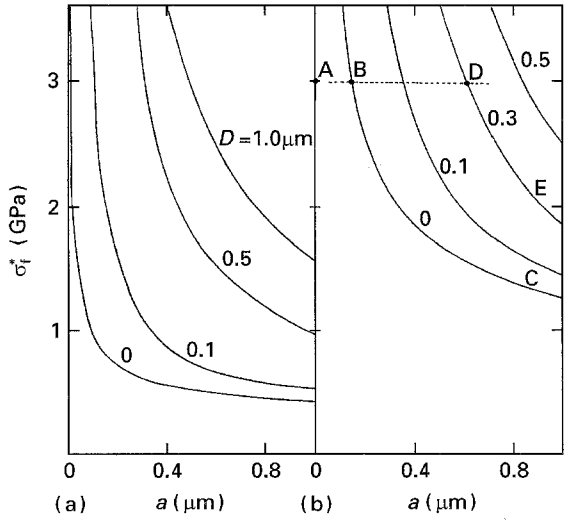

Figure 7 Influence of interfacial debonding length, D, on the variation of fibre strength at $X = 0$, σ_f^*, as a function of thickness of the coating layer, a, for (a) $E_f = 200$ GPa and $E_c = 400$ GPa, and (b) $E_f = 400$ GPa and $E_c = 200$ GPa. Taking the case of $\sigma_{fu}^0 = 3$ GPa, $E_f = 400$ GPa and $E_c = 200$ GPa, the practical fibre strength at $X = 0$ varies along ABC when no interfacial debonding occurs ($D = 0$), but it varies along ADE when the debonding length is 0.3 μm.

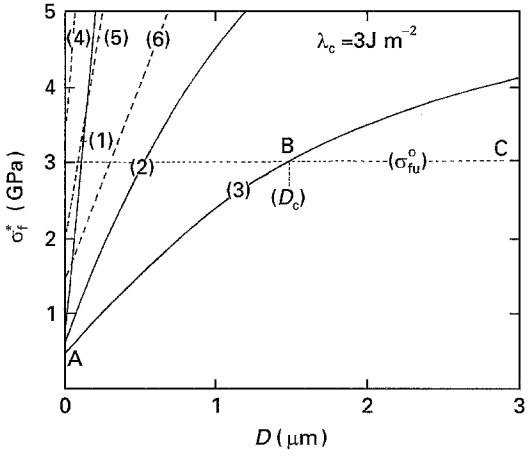

Figure 8 Increase in fibre strength at $X = 0$ with increasing interfacial debonding length D. Taking the case of $\sigma_{fu}^0 = 3$ GPa, $a = 0.6$, μm, $E_f = 200$ GPa and $E_c = 400$ GPa (curve 3), the practical σ_f^* value varies along ABC. In this case, beyond the critical debonding length at B, D_c, the fibre strength at $X = 0$ is given by σ_{fu}^0. Curves 1–6 as in Fig. 4.

a function of thickness of the coating layer a for (a) $E_f = 200$ GPa and $E_c = 400$ GPa, and (b) $E_f = 400$ GPa and $E_c = 200$ GPa. Fig. 8 shows the variation of σ_f^* with increasing interfacial debonding length, D. Figs 7 and 8 show that (i) the longer the debonding length, D, the higher becomes σ_f^* for a given thickness, a, (ii) σ_f^* decreases with increasing a for a fixed interfacial debonding length, and (iii) when the ratio of E_c/E_f is high, σ_f^* is low for given values of a and D.

The calculated values of σ_f^*, however, do not correspond to practical values, because in the range of $\sigma_f^* > \sigma_{fu}^0$ (original fibre strength without coating layer), the fibre stress at fracture is determined by the

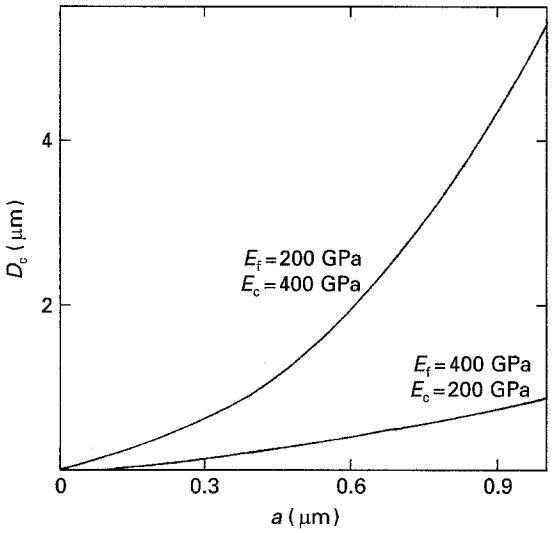

Figure 9 Variation of the critical debonding length, D_c, as a function of thickness of the coating layer, a, for case A, $E_f = 200$ GPa and $E_c = 400$ GPa, and for case B, $E_f = 400$ GPa and $E_c = 200$ GPa.

intrinsic defects contained in the fibre as stated in Section 4.2.1. Taking the case of $\sigma_{fu}^0 = 3$ GPa, $E_f = 400$ GPa and $E_c = 200$ GPa in Fig. 7b as an example, because σ_f^* is higher than σ_{fu}^0 up to B and D for $D = 0$ and 0.3 μm, respectively, the practical σ_f^* value cannot exceed the σ_{fu}^0 value. In these ranges, σ_f^* is given by σ_{fu}^0. As a result, the practical σ_f^* varies along ABC when no interfacial debonding occurs ($D = 0$) and it varies along ADE when debonding length is 0.3 μm.

Also taking the case of $\sigma_{fu}^0 = 3$ GPa, $a = 0.6$ μm, $E_f = 200$ GPa and $E_c = 400$ GPa (curve 3 in Fig. 8), the practical σ_f^* value varies along ABC. In this case, the debonding length at B corresponds to the critical debonding length D_c, below which practical value of σ_f^* is given by σ_{fu}^0. Fig. 9 shows the variation of D_c as a function of thickness of the coating layer a for case (A) $E_f = 200$ GPa and $E_c = 400$ GPa, and for case (B) $E_f = 400$ GPa and $E_c = 200$ GPa. It is suggested that, the thicker the coating layer, the longer the debonding length which is required to recover the strength of fibre, especially when the elastic modulus of the coating layer is higher than that of the fibre.

5. Conclusions

1. The energy release rate decreases with increasing debonding length. It is emphasized that the energy release rate is effectively reduced by small-scale debonding.

2. The energy release rate increases with increasing thickness of the coating layer for a given debonding length.

3. The higher the ratio of Young's modulus of the coating layer to that of the fibre, the higher the energy release rate becomes.

4. The strength of fibre at $X = 0$ increases with increasing debonding length below a critical debonding length, beyond which it is given by the original fibre strength.

Acknowledgement

The authors thank The ministry of Education Science and Culture of Japan for the Grant-in-Aid (no. 06452320).

References

1. A. G. METCALFE and M. J. KLEIN, in "Interface in Metal Matrix Composites", edited by A. G. Metcalfe (Academic Press, New York, 1974) pp. 125–68.
2. J. A. DICARLO, in "Proceedings, Mechanical Behaviour of Metal/Matrix Composites", edited by J. E. Hack and M. F. Amateau (AIME, Worrendale, PA, 1983) pp. 1–14.
3. S. OCHIAI, K. OSAMURA and Y. MURAKAMI, in "Progress in Science and Engineering of Composites", edited by T. Hayashi, K. Kawata and S. Umekawa, (Japan Society for Composite Materials, Tokyo, 1982) pp. 1331–8.
4. I. H. KHAN, *Metall. Trans.* **7A** (1976) 1281.
5. W. H. HUNT Jr, in "Interfaces in Metal-Matrix Composites", edited by A. K. Dhingra and S. G. Fishman (Metallurgical Society, Warrendale, PA, 1986) pp. 3–25.
6. M. Kh. SHOROSHOROV, L. M. USTINOV, A. M. ZIRLIN, V. I. OLEFILENKO and L. V. VINOGRADOV, *J. Mater. Sci.* **14** (1979) 1850.
7. S. OCHIAI, S. URAKAWA, K. AMEYAMA and Y. MURAKAMI, *Metall. Trans.* **11A** (1980) 525.
8. S. OCHIAI and K. OSAMURA, *J. Mater. Sci.* **23** (1988) 886.
9. *Idem, Metall. Trans.* **21A** (1990) 971.
10. H. TADA, P. C. PARIS and G. R. IRWIN, in "The Stress Analysis Handbook", edited by H. Tada, P. C. Paris and G. R. Irwin (Del Research Corporation, Hellertown, PA, 1973) pp. 1–31.
11. J. M. HEDGEPETH, NASA TN D-882 (1961).
12. S. OCHIAI and K. OSAMURA, *J. Mater. Sci.* **24** (1989) 3865.
13. C. ZWEBEN, *Eng. Frac. Mech.* **6** (1974) 1.
14. E. D. REEDY Jr, *Mech. Phys. Solids* **28** (1980) 265.
15. J. G. GOREE and R. S. GROSS, *Eng. Fract. Mech.* **13** (1980) 563.
16. J. A. NARIN, *J. Compos. Mater.* **22** (1988) 561.
17. H. FUKUDA, in "Achievement in Composites in Japan and the United States", Proceedings of Japan–US CCM-V, edited by A. Kobayashi (Japan Society for Composite Materials, Tokyo, 1990) pp. 529–34.
18. N. F. DOW, GEC Missile and Space Division, Report R63SD61, quoted by G. S. Holister and C. Thomas, in "Fiber Reinforced Materials" (Elsevier, London, 1966) p. 23.

Received 28 April
and accepted 23 November 1995